Author version: *Geophys. Res. Lett., vol.40(21); 2013; 5740-5744*

Origins of wind-driven intraseasonal sea level variations in the North Indian Ocean coastal waveguide

I. Suresh[1], J. Vialard[2], M. Lengaigne[2], W. Han[3], J. McCreary[4], F. Durand[5], P.M. Muraleedharan[1]

1. CSIR-National Institute of Oceanography, Goa, India

2. LOCEAN, IRD/CNRS/UPMC/MNHN, Paris, France

3. Dept. Of Atmospheric and Oceanic Sciences, University of Colorado, Boulder, USA

4. IPRC/SOEST, Univ. Hawaii, Hawaii, USA

5. LEGOS, IRD/CNES/UPS, Toulouse, France

Corresponding author address:

I. Suresh
CSIR-National Institute of Oceanography, Dona Paula – Goa 403 004 INDIA
E-mail: isuresh@nio.org

Abstract

In this paper, we show that a linear, continuously stratified ocean model reproduces observed wind-driven intraseasonal sea level variability in the coastal waveguide of the Northern Indian Ocean (NIO). Sensitivity experiments with intraseasonal wind forcing selectively applied in the equatorial region, Bay of Bengal, and Arabian Sea show that a large part of the basin-scale sea level variations are driven by zonal-wind fluctuations along the equator. Within the NIO coastal waveguide, the contribution of remote equatorial forcing decreases from ~80−90% in the Andaman Sea, to ~50% northeast of Sri Lanka and then increases to ~60−70% along the west coast of India. During the Southwest Monsoon, intraseasonal wind variations become stronger over the NIO, resulting in a larger contribution of local wind forcing to sea-level variability along the west (up to 60%) and east (up to 40%) coasts of India.

1. Introduction

The Asian continent bounds the Indian Ocean to the north. This distinct geographical setting drives the strongest monsoon on Earth, associated with seasonally reversing winds. These wind variations drive seasonal equatorial Kelvin and Rossby wave responses. The seasonal equatorial Kelvin waves propagate into the North Indian Ocean (hereafter NIO) as coastal Kelvin waves [*McCreary et al.*, 1993]. As a result, both local and remote forcing shape the seasonal variations of the East India Coastal Current [*Shankar et al.,* 1996; *McCreary et al.*, 1996]. A similar remote influence of equatorial wind forcing on the NIO sea level variability has also been demonstrated at interannual [e.g., *Han and Webster*, 2002] and decadal [*Nidheesh et al.*, 2013] timescales.

Indian Ocean winds also exhibit strong variability at intraseasonal timescales. In boreal winter, those wind variations are the strongest between the equatorial strip and southern tropics. They are associated with the Madden-Julian oscillation (hereafter MJO) [*Zhang*, 2005], a basin-scale atmospheric convective perturbation with ~30−80-day timescales. In boreal summer, intraseasonal variability (hereafter ISV) shifts northward and is associated with active and break phases of the Indian Summer Monsoon with ~30−60-day timescales [e.g., *Goswami,* 2005].

The MJO and active/break monsoon phases both have equatorial signatures, inducing ISV in the equatorial zonal-wind field throughout the year. The equatorial oceanic response to that wind variability has been described in many articles [e.g., *Masumoto et al.*, 2005; *Sengupta et al.*, 2007; *Iskandar and McPhaden,* 2011; *Nagura and McPhaden,* 2012]. On the other hand, only a few papers have focussed on NIO oceanic ISV. *Durand et al.* [2009] attributed ISV along the east coast of India to mesoscale eddies, which indeed contribute to variability in the interior Bay of Bengal [e.g., *Cheng et al.*, 2013]. Using satellite observations, *Vialard et al.* [2009] showed that the intraseasonal equatorial Kelvin waves propagate into the NIO in the form of coastal Kelvin waves. This study established a clear link between the equatorial and coastal waveguides in the NIO at intraseasonal timescales, as was earlier demonstrated at lower frequencies. Analysis of current-meter measurements on the west coast of India indicated that remote forcing contributes significantly to the variability of observed currents at intraseasonal timescales [*Shetye et al.*,2008; *Amol et al.,* 2012]. *Girishkumar et al.* [2013] further suggested that remote equatorial winds could also significantly influence intraseasonal thermocline variations observed in the interior of the Bay of Bengal, especially in the low-frequency tail of the intraseasonal band. These studies, however, did not precisely quantify the relative effects of remote and local forcing, particularly within the NIO coastal waveguide.

In this paper, our objective is to quantify the relative contributions of remote forcing from the equator and local forcing in the Bay of Bengal and Arabian Sea to intraseasonal sea level variations in the NIO coastal waveguide. In Section 2, we describe the linear ocean model, and the sensitivity experiments that allow us to evaluate the aforementioned contributions. We quantify these contributions in Section 3, and discuss their seasonality along the Indian coast. Section 4 provides a summary and discussion.

2. The linear continuously-stratified ocean model

We use a modified version of the linear, continuously stratified ocean model presented in detail in *McCreary et al.* [1996]. Solutions are represented as a sum of vertical normal modes, and are obtained numerically on a 0.25° regular grid over the 30°S−30°N, 30°E−110°E domain, with a coastline determined from the 200-m isobath. The model is forced by intraseasonal (20−150-day filtered) daily QuikSCAT wind-stresses (available from http://cersat/ifremer.fr/data/) from August, 1999 to October, 2009. Several studies indicate that this wind-stress product yields a realistic intraseasonal oceanic response in the equatorial Indian Ocean [e.g., *Sengupta et al.*, 2007; *Nagura and McPhaden,* 2012]. We show results obtained using 5 baroclinic modes but find, as in *Nagura and McPhaden* [2012] (see supplementary information), that the first 2 vertical modes dominate the equatorial sea-level solution, while the first mode dominates the sea-level solution north of 15°N in the NIO coastal waveguide. More details on the model are provided in the accompanying supplementary information.

We refer to the above solution as the control (CTL) experiment. To assess the relative importance of wind forcing in the equatorial (EQ), Bay of Bengal (BoB), Arabian Sea (AS), and southern Indian Ocean (SIO) regions, we perform sensitivity experiments by applying intraseasonal wind forcing only in each of those basins. The EQ region is bounded by 5^{o}N and 5^{o}S; the BoB and AS are confined to the north of 6^{o}N, and divided at 79.75^{o}E; the SIO is confined to the south of 6^{o}S (see Figure 2). The forcing in each sensitivity experiment is ramped down to zero within 1° of the borders of the forcing region, and the sum of all the forcings (i.e., EQ+BoB+AS+SIO) is equal to the forcing of CTL experiment. The linearity of the model then ensures that the sum of the sensitivity experiments is equal to the CTL solution.

We use 0.25° weekly sea levels (obtained from www.aviso.oceanobs.com/fr/accueil/index.html) to validate the model. Intraseasonal signals are obtained by applying a 20−150-day band-pass filter, after removing the mean seasonal cycle

computed from the first four harmonics. All analyses are based on 2001−2008 period (i.e., eight consecutive full years, after discarding the initial 1.5 years for adjustment of the model solutions).

3. Results

An empirical orthogonal function (EOF) analysis allows the main large-scale intraseasonal sea level pattern to be extracted in the model and observations. The first EOF is well separated from the rest of the variability in both observations (17% for first EOF shown in figure 1b, 6% for the second) and CTL experiment (44% for the first EOF shown in figure 1f, 14% for the second). Thus, this EOF captures the dominant large-scale intraseasonal sea level signal throughout the basin. The explained variance is larger in our linear model than in observations because the model does not produce eddies. The correlation of the model and observed sea level first principal component is 0.89, indicating that the linear model captures the phase of the observed basin-scale sea level variability remarkably well.

Figure 1 shows the wind stress and sea level patterns obtained from a lag-regression to the principal components (time series) associated with the first EOF. These patterns are remarkably similar to those shown in *Vialard et al.* [2009] and *Iskandar and McPhaden* [2011] though we used different method of analysis, indicating the robustness of these patterns. Equatorial westerly wind-stress anomalies force an equatorial downwelling Kelvin wave (Figures 1a,b) that reflects from the Sumatra coast as a downwelling equatorial Rossby wave (Figures 1c,d), with some of the energy propagating into and around the Bay of Bengal (Figures 1b,c) and up the west coast of India (Figure 1d) as coastal Kelvin waves. Figures 1e-h show that the CTL experiment captures the observed patterns remarkably well, both near the equator and in the coastal waveguide.

Most of the basin-scale variability is due to equatorial wind forcing, as shown by the good match in the basin-scale sea level pattern of the EQ solution with that of the observations and CTL (Figure 1i-l). We further quantify the point-wise contribution of forcing in each region by computing the regression coefficient of sea level in each sensitivity experiment to that in CTL (Figure 2). Note that this regression allows a general evaluation of the contribution of forcing in various regions to sea level ISV, not only to those associated with the first EOF shown in Figure 1. The SIO solution is negligible and hence not shown. With contributions of more than 95% (Figure 2a; coefficient values > 0.95), EQ wind forcing explains most of the sea level ISV within the equatorial waveguide, as has already been demonstrated in previous studies [e.g., *Nagura and McPhaden,* 2012]. The ISV amplitude of the EQ solution is larger than that of CTL near 5°N on both sides of the Maldives

archipelago (values slightly larger than 1 in Figure 2a). This feature is due to spurious Ekman pumping that occurs because ramping of the wind at 5°N in EQ artificially increases the wind-stress curl, but it has a negligible effect on our results (other solutions with a less abrupt ramping at the edge of the equatorial waveguide show qualitatively similar contributions).

The EQ contribution also dominates the solution in most of the NIO coastal waveguide. Around the rim of the Bay, the EQ contribution decreases from ~80−90% near Myanmar and in the Northern Bay down to ~50% north of Sri Lanka (Figure 2a). EQ forcing contributes to ~60−70% of the intraseasonal sea level variations along the west coast of India.

The EQ contribution expands westward offshore into the Bay of Bengal and Arabian Sea up to ~15°N, but is largely confined to the coast farther northward (Figure 2a). This trapping happens because first-baroclinic-mode Rossby waves exist only at periods longer than ~95 days north of 15°N [*Vialard et al.,* 2009], whereas the signals that originate from the equator have shorter periods [*Han*, 2005]. The progressive westward increase of the BoB and AS wind forcing to sea level ISV in the basin interiors (Figures 2b,c) is due to the contribution of local wind forcing to the Rossby waves as they propagate westward.

Wind-stress variations within the Bay contribute to sea level variations along the east coast of India through two processes: A) the arrival of Rossby waves generated in the basin interior, and B) the forcing by alongshore winds in the coastal waveguide. The southward-increasing contribution of BoB forcing along the east coast of India (Figure 2b) is likely due to a combination of those two processes. On the other hand, wind variations in the AS can only contribute to sea level ISV along the west coast of India through alongshore winds. The relatively constant value (~30%) of the AS contribution all along the west coast (Figure 2c) suggests that most of this alongshore wind forcing occurs near the southern tip of India.

Figure 3 shows the wind patterns associated with northern-hemisphere winter (panel a) and summer (panel b) basin-scale sea level ISV. The patterns are remarkably similar to the dominant modes of atmospheric variability: MJO in winter (e.g., *Zhang* [2005]) and active/break monsoon phases in summer (e.g., *Goswami* [2005]). While wind stress amplitude does not change much at the equator between the two seasons, it does become much larger over the NIO during summer (Figures 3a-b). Wind-stress curl is strong in the central and southern Bay of Bengal, and the alongshore wind stress is strong along the western rim of the Bay (Figure 3b). In the Arabian Sea, the winds are generally oriented perpendicular to the coast, except close to the southern tip of India and Sri Lanka

where they have a larger alongshore component, which is also associated with larger curl (Figure 3b).

The amplitude of the equatorial, remotely-driven, sea level ISV on both coasts of India does not change much between winter and summer (red bars on Figures 3c-d). Along the west coast of India, there is a large increase of wind-driven, sea level ISV in summer (blue bars, Figure 3c), likely linked to the larger alongshore wind-stress and curl variations close to the southern tip of India (Figure 3b). The WC box is representative of the west coast of India: the relative contributions of EQ and AS forcing do not vary much along this coast (not shown).

On the east coast of India, there is also a summer-time increase of the contribution in the Bay of Bengal forcing to sea level variations (green bars, Figure 3d). Alongshore wind stresses (Figure 3b) force downwelling coastal Kelvin waves that reinforce the remotely-driven sea level tendency (Figures 1i and j), while Ekman pumping in the central and southern Bay (Figure 3b) forces upwelling Rossby waves with the opposite contribution. Thus, the overall positive contribution of BoB forcing is due to the dominance of alongshore stresses along the western rim of the Bay. Similar analysis at other locations in the BoB coastal waveguide also indicates larger contribution of local forcing in summer. This contribution, however, diminishes when moving clockwise around the rim of the Bay.

The larger wind forcing results in larger variability (standard deviation) in NIO sea level during summer on both coasts of India (Figures 3c-d), with the proportion of regionally-forced to total sea level variability increasing from ~20% to ~40% on the west coast, and up to ~60% on the east coast.

4. Discussion

The observed intraseasonal, basin-scale, sea level patterns in the NIO identified by *Vialard et al.* [2009] are well reproduced by our wind-driven linear model. This validation gives us confidence to use the model to investigate the origins of wind-driven intraseasonal oceanic variations in the NIO, particularly in the coastal waveguide. Sensitivity experiments indicate that wind-forced, sea level variations in the NIO coastal waveguide are dominated by the contribution of equatorial-wind forcing. Around the rim of the Bay, this contribution decreases from ~80−90% in the Andaman Sea, to ~50% northeast of Sri Lanka and is ~60−70% along the west coast of India. The sea level variations along the coasts of Myanmar, Bangladesh and west coast of India can therefore be predicted several weeks in advance from sea level in the eastern equatorial Indian Ocean. Along the

east coast of India, eddy-induced ISV is large [e.g., *Durand et al.,* 2009] and can sometimes dominate the wind forced signal.

Our results further illustrate that the equatorial wind contribution to NIO sea level variations is modulated seasonally. The northward shift of the atmospheric ISV in summer induces larger fluctuations of alongshore wind stress on the western rim of the Bay and close to the southern tip of India. This increase results in larger sea level ISV, and a larger contribution of BoB and AS winds to this ISV, on both coasts of India during boreal summer.

Several previous studies [e.g., *Han,* 2005; *Iskandar and McPhaden,* 2011; *Girishkumar et al.,* 2013] have noted that the ocean's response to ISV forcing amplifies at longer periods (near 90-day) than the forcing itself (near 30−60 day). In this study, we chose to analyse these two frequencies together by using a 20−150-day filter, but the contributions of the various basins remain qualitatively similar when those two periods are considered separately (see supplementary information).

In the Bay of Bengal interior, *Girishkumar et al.* [2013] and *Cheng et al.* [2013] suggested a significant contribution of equatorial remote forcing. We consistently find that the equatorial solution contributes between 40 and 60% of the sea level ISV at the locations analysed by *Girishkumar et al.* [2013] (see supplementary information). Our results are also consistent with those of *Shetye et al.,* [2008] and *Amol et al.,* [2012], who suggested that remote forcing from farther south influences current variations along the west coast of India.

To our knowledge, the present study is the first one to quantifythe relative contributions of intraseasonal forcing in various regions of the Indian Ocean to wind-driven sea level ISV in the NIO coastal waveguide. Some issues, however, remain unresolved. Is alongshore wind stress ISV near the southern tip of India and along the western rim of the BoB the main source of coastal sea level local-forcing in summer, as suggested by this study? Is there vertical propagation of energy at intraseasonal timescales in the coastal waveguide, as suggested by *Nethery and Shankar* [2007] and *Amol et al.* [2012]? These topics will be investigated in a future study.

Acknowledgements: IS thanks S. Neetu, S.W.A. Naqvi, and T. Pankajakshan for their encouragement and acknowledges financial support from INCOIS/MoES under the INDOMOD program and of Council of Scientific and Industrial Research, New Delhi, India. JV, ML and FD are funded by Institut de Recherche pour le Développement (IRD). WH is supported by NOAA NA11OAR4310100. This research has been funded by the CNES AltiKa project. This work was

initiated while JV and ML were visiting scientists at CSIR-National Institute of Oceanography. This is NIO contribution number XXXX.

References

Amol, P., D. Shankar, S. G. Aparna, S. S. C. Shenoi, V. Fernando, S. R. Shetye, A. Mukherjee, Y. Agarvadekar, S. Khalap, and N. P. Satelkar(2012), Observational evidence from direct current measurements for propagation of remotely forced waves on the shelf off the west coast of India, *J. Geophys. Res.*, **117**, C05017, doi:10.1029/2011JC007606.

Cheng, X., S.-P. Xie, J.P. McCreary, Y. Qi, and Y. Du (2013), Intraseasonal variability of sea surface height in the Bay of Bengal, *J. Geophys. Res.*, **118**, 816-830, doi:10.1002/jgrc.20075.

Durand, F., D. Shankar, F. Birol, and S. S. C. Shenoi (2009), Spatio temporal structure of the East India Coastal Current from satellite altimetry, J. *Geophys. Res.*, **114**, C02013, doi:10.1029/2008JC004807.

Girishkumar, M. S., M. Ravichandran, and W. Han (2013), Observed intraseasonal thermocline variability in the Bay of Bengal, *J. Geophys. Res. Oceans,***118,** doi:10.1002/jgrc.20245.

Goswami, B. N. (2005), South Asian monsoon, in Intraseasonal Variability in the Atmosphere-Ocean Climate System, edited by W. K. M. Lau andD. E. Waliser, pp. 19– 55, Springer, Berlin.

Han, W. (2005), Origins and dynamics of the 90-day and 30– 60-day variations in the equatorial Indian Ocean, *J. Phys. Oceanogr.*,**35**, 708–728,doi:10.1175/JPO2725.1.

Han, W., and P.J. Webster (2002), Forcing mechanisms of sea level interannual variability in the Bay of Bengal, *J. Phys. Oceanogr.*,**32**, 216-239.

Iskandar, I., and M. J. McPhaden (2011), Dynamics of wind‐forced intraseasonal zonal current variations in the equatorial Indian Ocean, J. Geophys. Res., 116, C06019, doi:10.1029/2010JC006864.

Masumoto, Y., H. Hase, Y. Kuroda, H. Matsuura, and K. Takeuchi (2005), Intraseasonal variability in the upper layer currents observed in the eastern equatorial Indian Ocean, *Geophys. Res. Lett.*,**32**, L02607,doi:10.1029/2004GL021896.

McCreary, J. P., W. Han, D. Shankar, and S. R. Shetye (1996), Dynamics of the East India Coastal Current. 2. Numerical solutions. *J. Geophys. Res.*, **101**, 13993–14010, doi: 10.1029/96JC00560.

McCreary, J.P., Jr., P.K. Kundu, and R.L. Molinari (1993), A numerical investigation of dynamics, thermodynamics and mixed layer processes in the Indian Ocean, *Prog. Oceanogr.*,**31**, 181-244, doi:10.1016/0079-6611(93)90002-U

Nethery, D., and D. Shankar (2007), Vertical propagation of baroclinic Kelvin waves along the west coast of India, *J. Earth Syst. Sci.*, ***116***(4), 331–339, doi:10.1007/s12040-007-0030-6.

Nagura, M., and M. J. McPhaden (2012), The dynamics of wind-driven intraseasonal variability in the equatorial Indian Ocean, *J. Geophys. Res.*,**117,** C02001, doi:10.1029/2011JC007405.

Nidheesh, A.G., M. Lengaigne, J. Vialard, A.S. Unnikrishnan, and H. Dayan (2013), Decadal and long-term sea level variability in the topical Indo-Pacific Ocean, *Clim. Dyn.*,**41**, 381-402, doi:10.1007/s00382-012-1463-4

Sengupta, D., R. Senan, B. N. Goswami, and J. Vialard (2007), Intraseasonal variability of equatorial Indian Ocean zonal currents, *J. Clim.*,**20**, 3036– 3055, doi:10.1175/JCLI4166.1.

Shankar, D., J. P. McCreary, W. Han and S. R. Shetye (1996), Dynamics of the East India Coastal Current. 1: Analytic solutions forced by interior Ekman pumping and alongshore winds, *J. Geophys. Res.*,**101** (C6), 13975-13991.

Shetye, S. R., I. Suresh, D. Shankar, D. Sundar, S. Jayakumar, P.Mehra, R.G. Prabhudesai, and P. S. Pednekar (2008), Observational evidence for remote forcing of the West India Coastal Current, *J. Geophys. Res.*, **113**, C11001, doi:10.1029/2008JC004874.

Vialard, J., S. S. C. Shenoi, J. P. McCreary, D. Shankar, F. Durand, V. Fernando, and S. R. Shetye (2009), Intraseasonal response of the northern Indian Ocean coastal waveguide to the Madden-Julian Oscillation, *Geophys. Res. Lett.*,**36**, L14606, doi:10.1029/2009GL038450

Zhang, C. (2005), Madden-Julian Oscillation, *Rev. Geophys.*,**43**, RG2003,doi:10.1029/2004RG000158.

Figure captions

Figure 1: Lag-regression (Lags indicated on the middle column) of 20-150-day filtered QuikSCAT wind stress (first column) and sea level to the normalized principal component of the first EOF of 20-150-day filtered sea level in: a-d) observations (17% of total variance, second mode 6%), e-h) CTL experiment (44% of total variance, second mode 14%) and i-l) EQ experiment (49% of total variance, second mode 15%). The regression at lag 0 (panels b, f, and j) shows the spatial structure of the first EOF. Values that are not statistically significant at the 95% confidence level are masked (significance tests in this figure and figure 3 use a standard t-test, with one degree of freedom per 70 days of data, as determined from the lagged autocorrelation of the principal component used for the regression).

Figure 2: Contribution of wind forcing in the a) equatorial waveguide, b) Bay of Bengal, and c) Arabian Sea to intraseasonal sea-level variations, computed as the regression coefficients of 20-150-day filtered sea level of (a) EQ, (b) BoB, and (c) AS experiments to those of CTL experiment. The sum of the contributions is equal to 1 by construction (the Southern Indian Ocean contribution is negligible in the NIO). The dotted lines indicate the boundaries of the domain in which the EQ, BoB, and AS forcing are applied.

Figure 3: 20-150-day filtered QuikSCAT wind stress (vectors) and wind stress curl (colors) regressed to the normalized first principal component of 20-150-day filtered observed sea level at 14 day lead, for a) December-March and b) June-September. Decomposition of 20-150-day sea level standard deviation (cm, also indicated as a %) in the c) WC (west coast; 73.5°E-74.5°E, 12°N-13°N, cf panel a) and d) EC (east coast; 80.5°E-81.5°E, 13°N-14°N; cf panel b) boxes into contributions from equatorial (red), Bay of Bengal (green), Arabian Sea (blue), and South Indian Ocean (orange) wind forcing, for DJFM and JJAS. The -14 day lag was selected for this plot, because it is associated with the largest wind stress and wind stress curl perturbations.

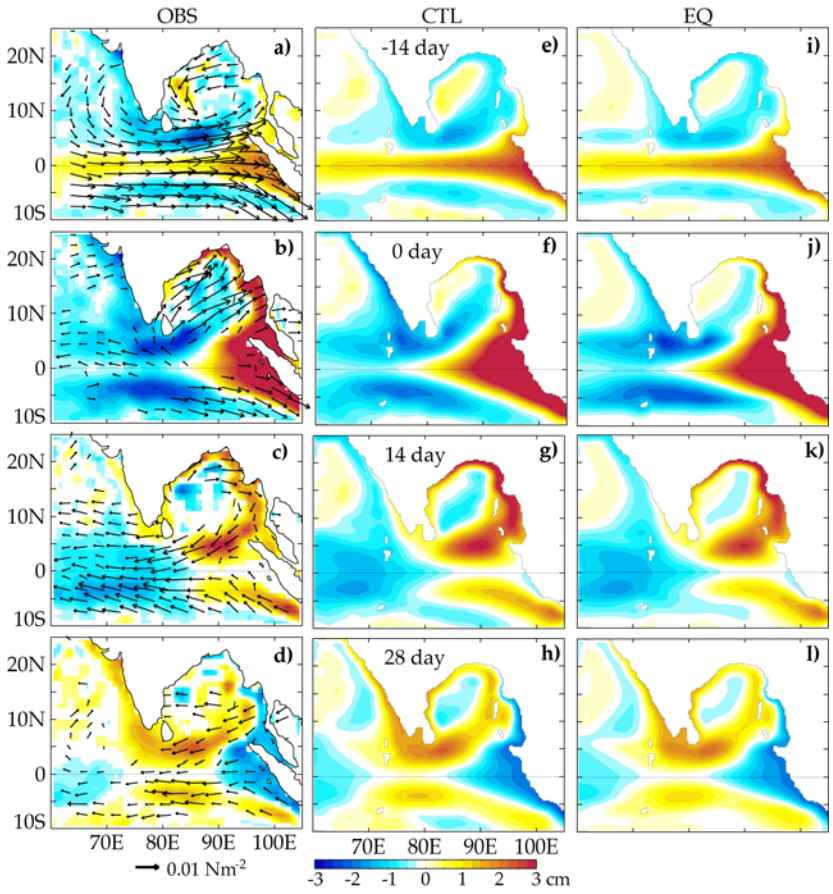

Figure 1: Lag-regression (Lags indicated on the middle column) of 20-150-day filtered QuikSCAT wind stress (first column) and sea level to the normalized principal component of the first EOF of 20-150-day filtered sea level in: a-d) observations (17% of total variance, second mode 6%), e-h) CTL experiment (44% of total variance, second mode 14%) and i-l) EQ experiment (49% of total variance, second mode 15%). The regression at lag 0 (panels b, f, and j) shows the spatial structure of the first EOF. Values that are not statistically significant at the 95% confidence level are masked (significance tests in this figure and figure 3 use a standard t-test, with one degree of freedom per 70 days of data, as determined from the lagged autocorrelation of the principal component used for the regression).

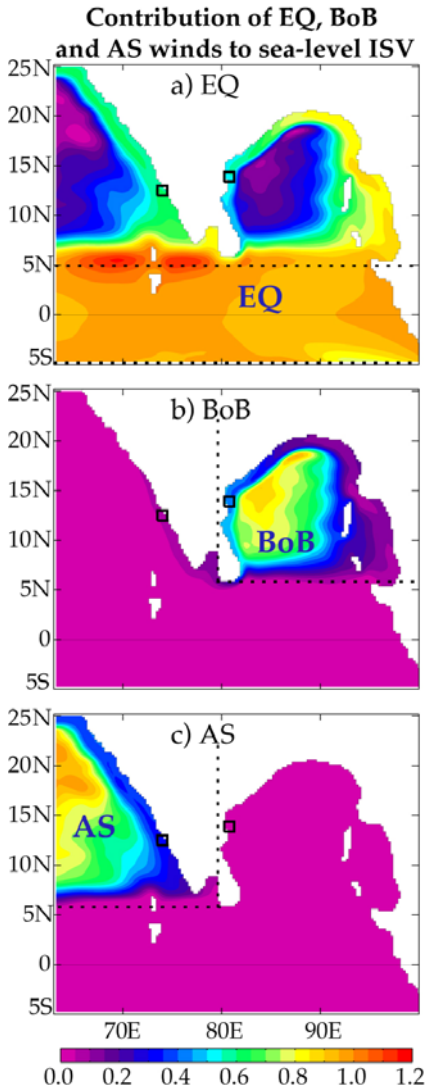

Figure 2: Contribution of wind forcing in the a) equatorial waveguide, b) Bay of Bengal, and c) Arabian Sea to intraseasonal sea-level variations, computed as the regression coefficients of 20-150-day filtered sea level of (a) EQ, (b) BoB, and (c) AS experiments to those of CTL experiment. The sum of the contributions is equal to 1 by construction (the Southern Indian Ocean contribution is negligible in the NIO). The dotted lines indicate the boundaries of the domain in which the EQ, BoB and AS forcing are applied.

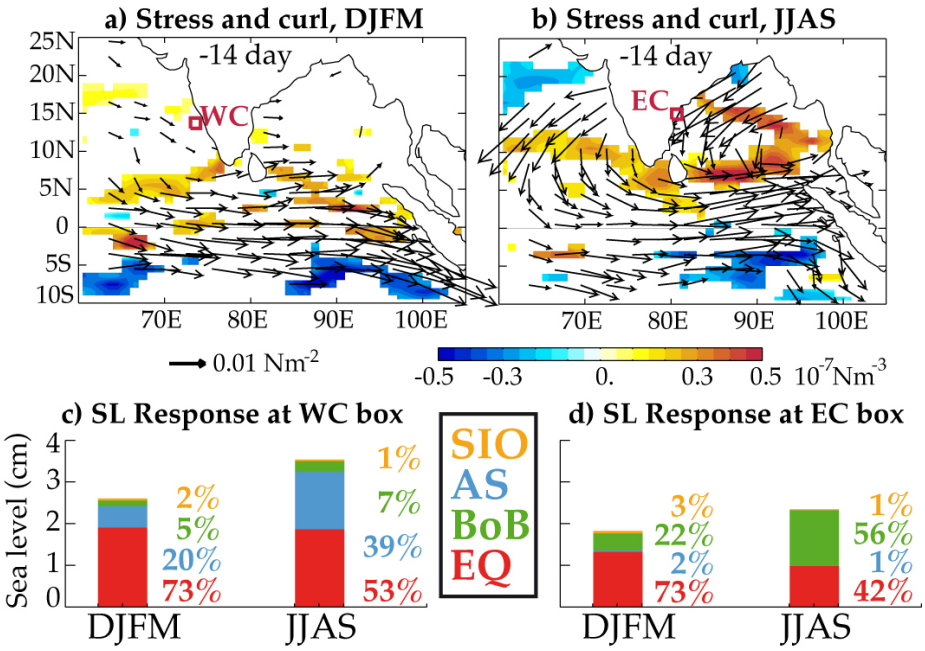

Figure 3: 20-150-day filtered QuikSCAT wind stress (vectors) and wind stress curl (colors) regressed to the normalized first principal component of 20-150-day filtered observed sea level at 14 day lead, for a) December-March and b) June-September. Decomposition of 20-150 day sea level standard deviation (cm, also indicated as a %) in the c) WC (west coast; 73.5°E-74.5°E, 12°N-13°N, cf panel a) and d) EC (east coast; 80.5°E-81.5°E, 13°N-14°N; cf panel b) boxes into contributions from equatorial (red), Bay of Bengal (green), Arabian Sea (blue), and South Indian Ocean (orange) wind forcing, for DJFM and JJAS. The -14 day lag was selected for this plot, because it is associated with the largest wind stress and wind stress curl perturbations.

Supplementary information to "***Origins of wind-driven intraseasonal sea level variations in the North Indian Ocean coastal waveguide***" by Suresh et al.

1. The linear, continuously stratified ocean model

We use a modified version of the linear, continuously stratified ocean model presented in detail in *McCreary et al.* [1996]. The equations of motion are linearized about a state of rest with a realistic background stratification obtained from the averaged (15^oS-15^oN, 40^oE-100^oE) World Ocean Atlas (WOA09) [*Locarnini et al.*, 2010] climatological potential density profile, and the ocean bottom is assumed flat. Solutions are represented as a sum of vertical normal modes of the system. We hence use 5 baroclinic modes, the characteristic speeds of which are 252 cm s^{-1},155 cm s^{-1}, 88 cm s^{-1}, 69 cm s^{-1}, and 53 cm s^{-1}. The response of each mode is obtained on a regular grid with a resolution of 0.25°. The domain extends from 30°S to 30°N and from 30°E to 110°E, and has a coastline determined by the 200-m isobaths [*Smith and Sandwell*, 1997].

Vertical mixing has the same form as *McCreary et al.* [1996], but with a 12-month dissipation time scale for the first baroclinic mode as in *Nagura and McPhaden* [2012], which implies a ~5 month dissipation timescale for the second baroclinic mode. The horizontal mixing coefficient is set to 5000 m^2 s^{-1}. Wind is introduced into the ocean as a body force with the same profile (constant down to 50 m and ramped to zero at 100 m) as *McCreary et al.* [1996].

The model is forced by intraseasonal (20-150-day filtered) daily QuikSCAT wind-stresses (available from http://cersat/ifremer.fr/data/) from August, 1999 to October, 2009. QuikSCAT wind forcing has been used in many studies of the tropical Indian Ocean intraseasonal variability [e.g., *Senan et al.*, 2003; Sengupta *et al.*, 2007; *Nagura and McPhaden*, 2012], with an oceanic response in good agreement with observations.

We refer to the above solution as the control (CTL) experiment.

2. Contributions from Baroclinic Modes

The solution of the linear model is well converged using only the first 5 modes (with almost identical results with first 20 modes). In fact, the first two modes contribute to more than 90 % of the sea level solution everywhere, except in a narrow equatorial strip (figure S1 below). Even in this narrow band, first 2 modes explain more than 80% of the 20-modes solution, in agreement with the results of *Nagura and McPhaden* [2012], who show that the first 2 baroclinic modes are sufficient to reproduce the equatorial intraseasonal variability in

the Indian Ocean.

In the Northern Indian Ocean coastal waveguide, the first mode is generally sufficient to explain most of the variability, except south of 15°N in the Andaman Sea and eastern Arabian Sea. While Mode 2 explains between 20 and 30% of the solution in the equatorial waveguide, it explains at most 20%, and often less than 10% in the coastal waveguide. The Rossby radius for the second baroclinic mode falls below 50 km (i.e., 2 gridpoints) north of 12°N, and mode 2 will vanish because of insufficient resolution and numerical dissipation.

Since mode 2 plays a smaller role in the coastal waveguide than at the equator, vertical energy propagation will be more limited in our model's coastal waveguide than diagnosed at the equator [*Iskandar and McPhaden,* 2011] from observations. The co-existence of modes 1 and 2 south of 15°N along the west coast of India will however allow some vertical energy propagation there, in agreement with observations from [*Amol et al.,* 2012].

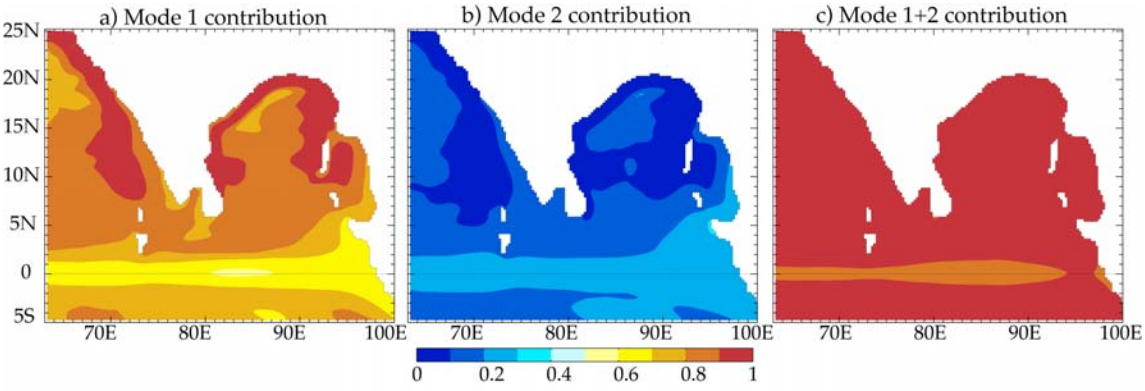

Figure S1: Regression coefficient of a) first, b) second and c) first two baroclinic modes sea level to the solution obtained from the first 20 modes.

3. Sensitivity of the results to the timescale

While intraseasonal wind stress forcing displays most energy in the 30-60 day window, the oceanic sea level response in general displays more energy near the 90 day timescale [e.g. *Han,* 2005; *Girishkumar et al.,* 2013]. This has been attributed to the occurrence of resonant response of the Indian Ocean basin to wind forcing, near the 90-day period [e.g., *Han*, 2005; *Han et al.* 2011].

In our study, we chose not to distinguish between those two frequencies, but consider them as a whole, by filtering the results in the 20-150-day window. Figure S2, below, is identical to Figure 2 of the paper, but this time produced selectively for two frequency bands encompassing the main forcing period (30-70 day) and the 90-day response (70-110 day).

Supplementary information to "***Origins of wind-driven intraseasonal sea level variations in the North Indian Ocean coastal waveguide***" by Suresh et al.

Inside the equatorial and northern Indian Ocean coastal waveguide, the contributions of the various regions in Figure S2 are remarkably similar to those obtained in the paper. There is however a larger contribution of EQ forcing in the 70-110-day band in the eastern AS and BoB basins, because offshore radiation of coastal signals by planetary wave can occur further north at lower frequency [e.g., *Vialard et al.*, 2009].

At 90 day, the equatorial solution contributes to 40-60% of the sea level variations at the locations analysed by *Girishkumar et al.*, [2013], consistent with their statement that "*The near 90 day and 120 day thermocline variability is driven primarily by the variability of equatorial zonal wind stress.*"

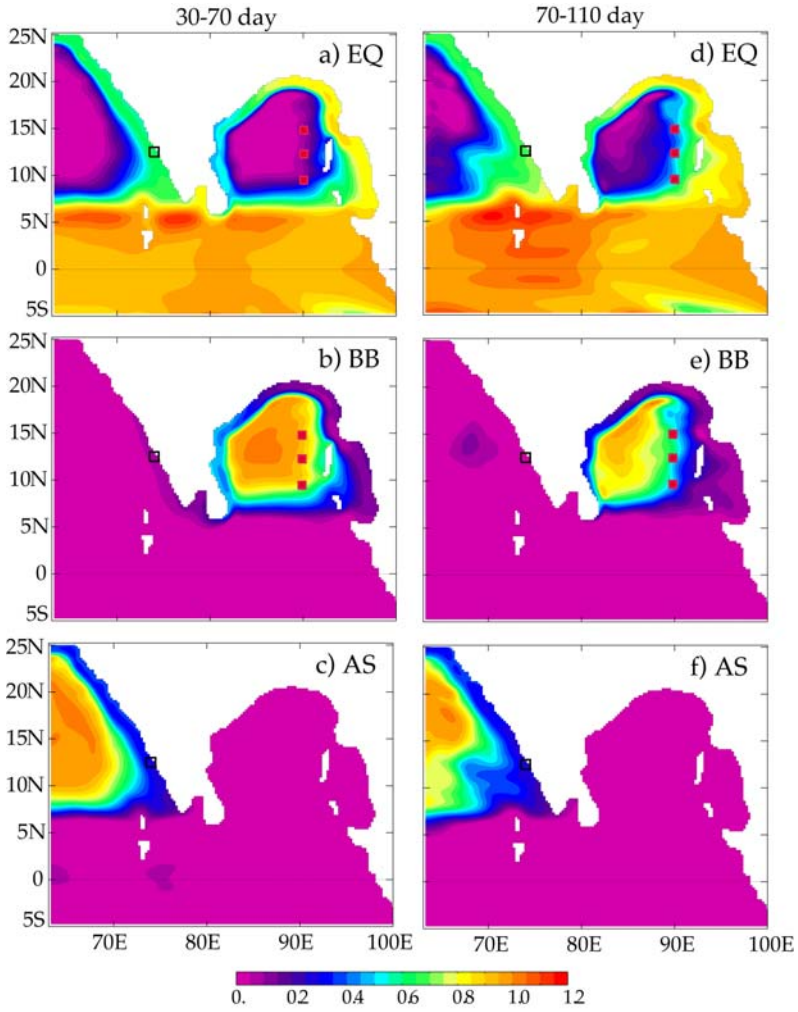

Figure S2: Same figure as Figure 2 of the paper, but for the 30-70 and 70-110-day bands separately. The colours represent the contribution of wind forcing in the EQ, BoB and AS regions, computed as the regression coefficients of 30-70 or 70-110-day filtered sea level of (a) EQ, (b) BoB, and (c) AS experiments to that of CTL experiment. The sum of the contributions is equal to 1 by construction. The filled red squares indicate the locations of the 8°N, 12°N and 15°N RAMA moorings at 90°E.

References

Amol, P., D. Shankar, S. G. Aparna, S. S. C. Shenoi, V. Fernando, S. R. Shetye, A. Mukherjee, Y. Agarvadekar, S. Khalap, and N. P. Satelkar (2012), Observational evidence from direct current measurements for propagation of remotely forced waves on the shelf off the west coast of India, *J. Geophys. Res.*, **117**, C05017, doi:10.1029/2011JC007606.

Girishkumar, M. S., M. Ravichandran, and W. Han (2013), Observed intraseasonal thermocline variability in the Bay of Bengal, *J. Geophys. Res. Oceans*, **118,** doi:10.1002/jgrc.20245.

Han, W. (2005), Origins and dynamics of the 90-day and 30–60 day variations in the equatorial Indian Ocean, *J. Phys. Oceanogr.*, **35,** 708–728.

Han, W., J. P. McCreary, Y. Masumoto, J. Vialard and B. Duncan, 2011 : Basin modes in the equatorial Indian Ocean, *J. Phys. Oceanogr.*,**41,** 1252-1270.

Iskandar, I., and M. J. McPhaden (2011), Dynamics of wind□forced intraseasonal zonal current variations in the equatorial Indian Ocean, *J. Geophys. Res.*, **116**, C06019, doi:10.1029/2010JC006864.

McCreary, J. P., W. Han, D. Shankar, and S. R. Shetye (1996), Dynamics of the East India Coastal Current. 2. Numerical solutions. *J. Geophys. Res.*, **101**, 13993–14010, doi: 10.1029/96JC00560.

Locarnini, R. A., A. V. Mishonov, J. I. Antonov, T. P. Boyer, H. E. Garcia, O. K. Baranova, M. M. Zweng, and D. R. Johnson (2010), World Ocean Atlas 2009, Volume 1: Temperature. S. Levitus, Ed. NOAA Atlas NESDIS 68, U.S. Government Printing Office, Washington, D.C., 184 pp.

Nagura, M., and M. J. McPhaden (2012), The dynamics of wind-driven intraseasonal variability in the equatorial Indian Ocean, *J. Geophys. Res.*, **117,** C02001, doi:10.1029/2011JC007405.

Senan, R., D. Sengupta, and B. N. Goswami (2003), Intraseasonal ''monsoon jets'' in the equatorial Indian Ocean, *Geophys. Res. Lett.*, **30** (14), 1750, doi:10.1029/2003GL017583, 2003.

Sengupta, D., R. Senan, B. N. Goswami, and J. Vialard (2007), Intraseasonal variability of equatorial Indian Ocean zonal currents, *J. Clim.*, **20**, 3036– 3055, doi:10.1175/JCLI4166.1.

Smith, W.H. F., and D.T., Sandwell (1997), Global sea floor topography from satellite altimetry and ship depth soundings, *Science*, **277**, 5334.

Vialard, J., S. S. C. Shenoi, J. P. McCreary, D. Shankar, F. Durand, V. Fernando, and S. R. Shetye (2009), Intraseasonal response of the northern Indian Ocean coastal waveguide to the Madden-Julian Oscillation, *Geophys. Res. Lett.*, **36,** L14606, doi:10.1029/2009GL038450.